

www.advelectronicmat.de

Programmable Racetrack for Magnetic Domain Wall Motion via Local Tuning of Exchange Biased Field

Hyun-Joong Kim, Kyoung-Woong Moon, Seongsoo Yoon, Kyongmo An, Changsoo Kim, Seungmo Yang, Tae-Seong Ju, Jong Wan Son, Jung-Il Hong, and Chanyong Hwang*

To overcome memory bottleneck issues in memory-centric chip technologies, in-memory computing has been considered an alternative route involving simultaneous data storage and computing in a memory network. In the context of spintronics, a memory-in-logic device based on spin-transfer-torque or spin-orbit-torque magnetoresistive random-access memory, and a magnetic domain wall (DW) racetrack has been studied. To expand the functionalities of a conventional magnetic DW racetrack, the study devises a reprogrammable exchange-biased DW racetrack with local engineering of the exchange bias field ($H_{\rm E}$) in continuous magnetic films without requiring a lithography process for specific patterning of the films. Furthermore, current-driven and field-driven DW motion along the exchange-biased racetrack is demonstrated. Additionally, within the route of the locally different exchange-biased racetrack, a gate function can be performed to guide or stop DW motion by locally tuning $H_{\rm E}$. The complex maze racetrack is rewritable, and multiple input channels can be controlled.

1. Introduction

The magnetization state, as a collective manifestation of electron spin, can represent '1' and '0' for data storage devices. Despite the wide industrial use of magnets for data storage, fabricating a microprocessor using spin-based logic devices could pose a significant challenge. Recently, Jung et al.^[1] demonstrated in-memory computing architectures using a crossbar array. Allwood et al.^[2]

H.-J. Kim, K.-W. Moon, K. An, C. Kim, S. Yang, T.-S. Ju, J. W. Son, C. Hwang Quantum Technology Institute
Korea Research Institute of Standards and Science (KRISS)

267 Gajeong-ro, Daejeon 34113, Republic of Korea

E-mail: cyhwang@kriss.re.kr

S. Yoon, J.-I. Hong Department of Emerging Materials Science Daegu Gyeongbuk Institute of Science and Technology (DGIST) 333 Techno Jungang-Daero, Daegu 42988, Republic of Korea

The ORCID identification number(s) for the author(s) of this article can be found under https://doi.org/10.1002/aelm.202400027

© 2024 The Authors. Advanced Electronic Materials published by Wiley-VCH GmbH. This is an open access article under the terms of the Creative Commons Attribution License, which permits use, distribution and reproduction in any medium, provided the original work is properly cited.

DOI: 10.1002/aelm.202400027

devised a proof of concept of an in-plane field-driven domain wall (DW) logic for implementing various logic functions. Parkin et al.^[3] experimentally demonstrated an electric current-driven DW racetrack memory in a nanowire for information storage. Luo et al.^[4] have recently demonstrated electric logic operations in DW racetracks. Therefore, the use of logic operations as well as data storage based on DW racetracks has been drawing increased attention and is an essential task in spintronics.

An exchange-coupled antiferromagnet (AFM)/ferromagnet (FM) heterogeneous system has utilized the exchange bias effect for versatile functionalities in spintronic devices such as magnetic random-access memory (MRAM).^[5–10] The exchange-biased spin valve,^[11,12] involving the pinning of FM magnetization

combined with AFM, has been suggested as a representative system for developing the giant magnetoresistance or tunneling magnetoresistance phenomena in information storage devices.[9,13,14] The exchange bias effect manifests as a phenomenon in which the FM layer experiences an additional magnetic field due to the magnetization of the AFM layer, termed an exchange bias field (H_E) . In further studies, control of H_E has been achieved via the application of diverse external stimuli, including electric current, [15–19] electric field [20–22] mediated with piezoelectric strain, [23-26] or voltage-driven ion migration [27-29], and optical light with helicity.^[30] Recent studies^[3,31–33] on FM domain wall (DW) motion in AFM/FM systems have focused solely on $H_{\rm E}$ control, but manipulating DW motion through AFM magnetization control has been rarely studied. In our previous report,[34] we demonstrated FM DW motions influenced by spin current-induced AFM switching. This indicates that $H_{\rm F}$ is tunable and can influence DW motions.

In the present work, within an exchange-coupled bilayer system, we achieved a locally different exchange-biased (LDEB) DW racetrack and LDEB magnetic patterning in a continuous film through local reconfigurable engineering of $H_{\rm E}$, without conventional processes such as lithography, milling, and etching for permanent fabrication of wires, crossbars, or complex-patterned films. The local engineering of $H_{\rm E}$ was performed through localized field cooling (LFC) of the AFM magnetization. In previous reports, [35,36] local heating via laser

www.advelectronicmat.de

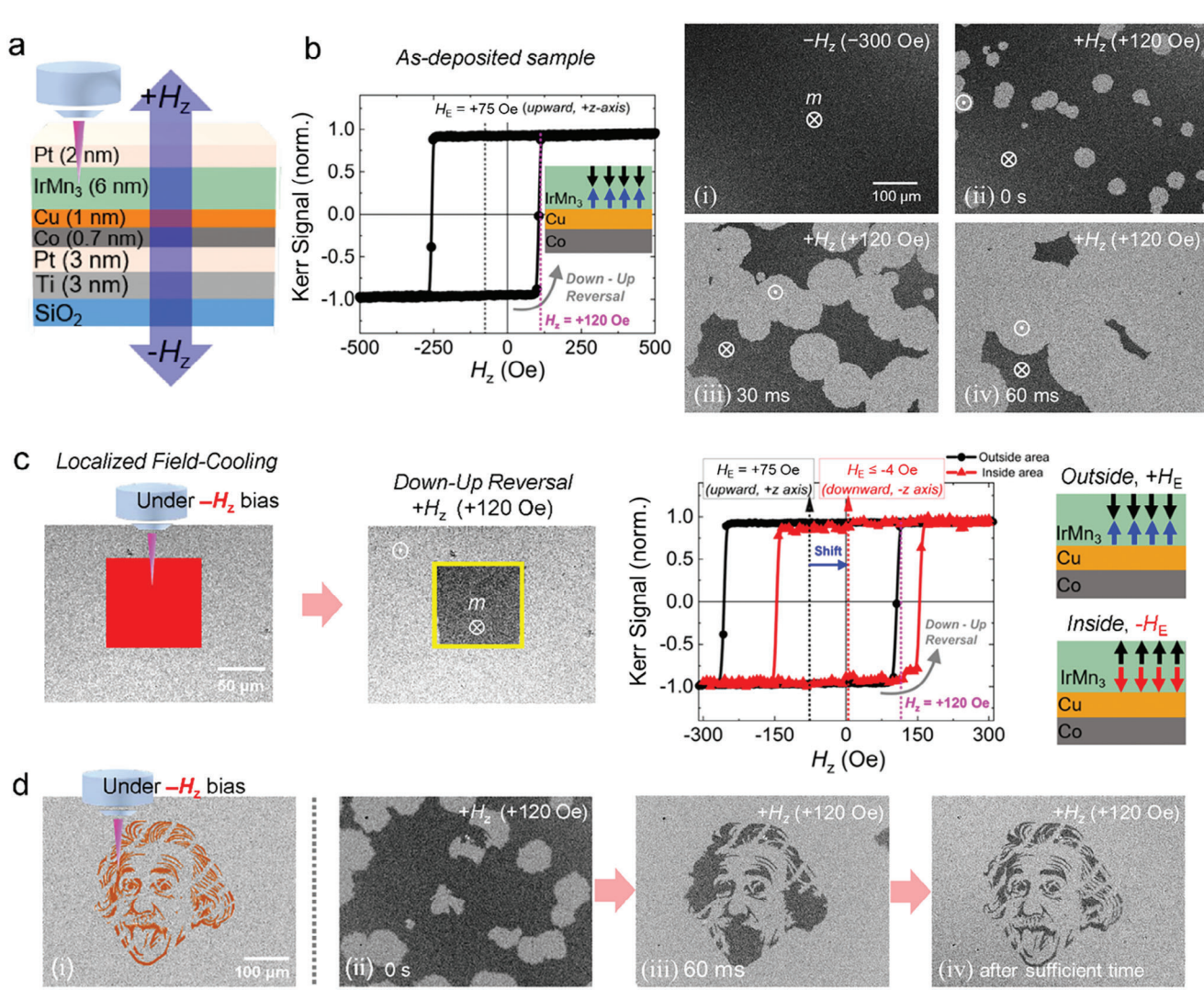


Figure 1. a) Schematic view of the continuous multilayer. The exchange-coupled FM/AFM bilayers with a Cu space layer between the bilayers consisting of Co (0.7 nm)/Cu (1 nm)/IrMn₃ (6 nm) were grown on Ti (3 nm)/Pt (3 nm) buffer layers on SiO₂ substrate with Pt (2 nm) capping layer and LFC treatment using laser heating under H_z bias. b) The as-deposited sample's magnetic hysteresis loop and MOKE images of magnetic domain expansion, the time interval of each image (ii–iv) is 30 ms, and the field-driven DW speed is ≈0.8 mm/s. m represents a normalized magnetization vector of the FM layer. c) Local engineering of H_E was achieved after LFC treatment at the red square (100 μm × 100 μm). d) 'Albert Einstein'-exchange biased magnetic patterning. In each image, Roman numerals indicate the sequence of state changes.

irradiation was shown to induce the AFM-FM transformation in FeRh film and enable control of the exchange-biased AFM/FM system.

Magnetic DW racetracks have garnered tremendous interest and are considered a new concept for memory and logic devices due to their advantages of nonvolatility, fast data processing, and high density. [2,4,37–44] Our local $H_{\rm E}$ engineering enables various types of LDEB DW racetracks, replacing conventional wirepatterned DW racetracks. Moreover, we achieved a function of the LDEB gate for halting or controlling the field- or current-driven DW motion in the LDEB racetrack. A multibranch or complex maze type of racetrack was rewritable in a continuous magnetic film, and multiple input channels could be created. Thus, our LDEB magnetic patterning can be expected to diversify and expand the functions of conventional DW devices.

2. Results and Discussion

2.1. Local Engineering of $H_{\rm E}$ via LFC Treatment

Multilayers of Ti (3 nm)/Pt (3 nm)/Co (0.7 nm)/Cu (1 nm)/IrMn₃ (6 nm)/Pt (2 nm) were deposited at room temperature on a ${\rm SiO}_2$ substrate by magnetron sputtering (**Figure 1**a). The depositions were achieved under a *z*-axis-oriented external magnetic field (H_z) along the upward-perpendicular direction (+*z*) with respect to the sample plane to establish a unidirectional and perpendicular H_E over the entire film surface. Consequently, the perpendicular magnetic hysteresis loop of the initial as-deposited sample was shifted by –75 Oe (Figure 1b). The magnitude of this loop shift can be obtained from the average value of the two coercive fields (120 Oe and –270 Oe in Figure 1b). This shift can be



www.advelectronicmat.de

interpreted as requiring H_z of –75 Oe to offset H_E of +75 Oe due to the +z direction of IrMn₃ AFM magnetic momentum at the interface between FM Co and AFM IrMn₃ with the 1-nm-thick Cu space layer. The role of the Cu space layer is to alleviate the strong and direct exchange coupling of the FM/AFM bilayers. Accordingly, as the thickness of the Cu space layer increases, the magnitude of H_E decreases (Figure S1, Supporting Information).

The magnetic images in Figure 1b observed by a magneto-optical Kerr effect (MOKE) microscope show how the magnetization reversal of the FM layer of the as-deposited sample occurred (see Experimental Section). The MOKE microscope was set up so that magnetization in the -z direction (down) appeared dark gray, and magnetization in the +z direction (up) appeared light gray. Initially, the entire magnetization of the FM layer was maintained in down-magnetization by negative H_z (Figure 1bi). When the H_z value was set to +120 Oe, circular up domains were nucleated and expanded (Figure 1bii–iv). Through this process, a down-up (from down to up) magnetization reversal of the FM layer was completed. Since the shape of the observed circular domains was point symmetrical, it can be seen that the magnetic properties in the observation area were uniform.

Typically, a realignment of the AFM magnetic moment via the field-cooling procedure is required for setting or resetting the $H_{\rm E}$. This involves heating the AFM above the Néel temperature (T_N) to overcome the existing anisotropy, followed by cooling in a magnetic field. Thus, our LFC procedure irradiated a focused laser light with a 35-mW power and 660-nm wavelength for 10 ms to heat a selected area of the sample. In general, the T_N of the IrMn₃ thick layer was reported to be ≈550 K.[45] The blocking temperature (TB) of the IrMn film depends on the thickness, [46] with reported values corresponding to 450 K for a 3.5-nm layer^[47] and 520 K for a 9.1-nm layer. ^[45] Thus, the $T_{\rm R}$ of the 6-nm-thick IrMn₃ layer used in the present work was expected to be between 450 and 520 K. To investigate whether the temperature of the surface area irradiated by the laser light increases above the $T_{\rm R}$, the temperature increase was simulated (see Figure S2, Supporting Information). The calculation yielded a temperature increase of over 550 K to realize the LFC procedure. Additionally, the calculation result showed that the temperature increase and decrease converged within 1 µs, so it is assumed that all experiments after LFC were performed under room temperature conditions (Figure S2c, Supporting Information).

Practically, switching the magnetic moment direction of IrMn₃ from upward to downward at the interface between Co and IrMn₃ requires applying a negative H_z bias during LFC. Therefore, the local area corresponding to the red square (100 μ m × 100 μ m) was heated by laser light under – H_z (\approx –200 Oe) bias (Figure 1c) (see Experimental Section for further details). As a result, at +120 Oe of H_z bias during the down-up reversal, the down magnetic domain (dark gray) is switched into an up domain (light gray) at the outside area of the yellow solid-lined box, while it still retains its down magnetization state at the inside area of the box (Figure 1c). From the two coercive fields (150 Oe and –142 Oe) obtained from the locally measured hysteresis loop, H_E in the LFC-treated area was estimated to be –4 Oe. However, obtaining H_E from the two coercive fields is not reliable when the sample uniformity is broken, and this will be discussed later.

The LFC via laser heating can change $H_{\rm E}$ locally, demonstrating the feasibility of an exchange-biased magnetic pattern within

continuous films. After local engineering of $H_{\rm E}$ with a specific pattern corresponding to the orange-color image of Albert Einstein (Figure 1di), the pattern maintained down magnetization even if other areas experienced the down-up magnetization reversal by +120 Oe of $H_{\rm z}$ (Figure 1dii–iv). In addition, despite repeated up-down or down-up magnetization reversals by applying negative or positive $H_{\rm z}$, the 'Albert Einstein image' of the exchange-biased magnetic pattern remained, indicating the possibility of use as a memory device.

Albisetti et al. [48] achieved local engineering of in-plane $H_{\rm E}$ in directly exchange-coupled IrMn/in-plane magnetic anisotropy CoFeB bilayers system via LFC using the hot tip of a scanning probe microscope (SPM). Additionally, in the article, it was demonstrated that spin-wave excitation and propagation were locally controlled in reconfigurable magnetic patterns via thermally assisted magnetic scanning probe lithography (tam-SPL). Similarly, our present work could locally control and reprogram a configuration of H_E via LFC by laser heating. To implement this, the local area as illustrated in Figure 1c was heated again by irradiating laser light under + H_z (\approx +200 Oe) bias. Additionally, to increase the accuracy of $H_{\rm F}$ measurement, a method was devised and used to find the H_{τ} value that stops all the DWs (see Experimental Section). Then, the $H_{\rm F}$ of the area was switched from -12Oe to +16 Oe as shown in Figure 2a. Furthermore, successive $H_{\rm E}$ switching was observed after LFC under positive and negative H_{π} bias (Figure 2b).

The imperfect $H_{\rm E}$ switching with a small magnitude might be induced by a lack of experimental laser heating overcoming $T_{\rm N}$ or $T_{\rm B}$ of AFM. Since the local area by LFC treatment is the size of the laser spot (\approx 2 μ m²), we used the laser scanning method for patterning a larger area. Consequently, there might be a different result of $H_{\rm E}$ switching between global and local field cooling treatments because the intensity of laser light has a Gaussian shape, which will cause uneven temperature distribution. To improve this phenomenon, an experimental system or material of the film needs to be optimized, including the irradiation of flattop laser light with high power under vacuum conditions or the replacement of AFM with low $T_{\rm N}$ or $T_{\rm B}$.

2.2. Writing-Erasing-Rewriting Function of LDEB Pattern

Using these successive $H_{\rm E}$ switching processes, the writingerasing-rewriting function of the LDEB pattern in an identical area was investigated (see Figure 2c). First, for the as-deposited sample, circular up-magnetic domains were nucleated and expanded under positive H_{z} (+120 Oe) bias. Then, the 1st process, corresponding to laser heating on an orange-colored pattern the 'cat in the box' – under $-H_z$ bias, was carried out. The 1st process left down-magnetic domains of the 'cat in the box' pattern during down-up reversal. Sequentially, the 2nd process was performed to remove only the cat from the 'cat in the box' pattern. The 2nd process involved heating the area in the red square covering the cat pattern under $+ H_z$ bias. As a result, during downup reversal under identical H_z (+120 Oe) bias, the empty boxpatterned domains remained. Finally, the 3rd process, laser heating on the orange-colored pattern - 'Albert Einstein' - with negative H_z , was done, and then he appeared in the empty box under identical H_z (+120 Oe) bias during down-up reversal. Therefore,





www.advelectronicmat.de

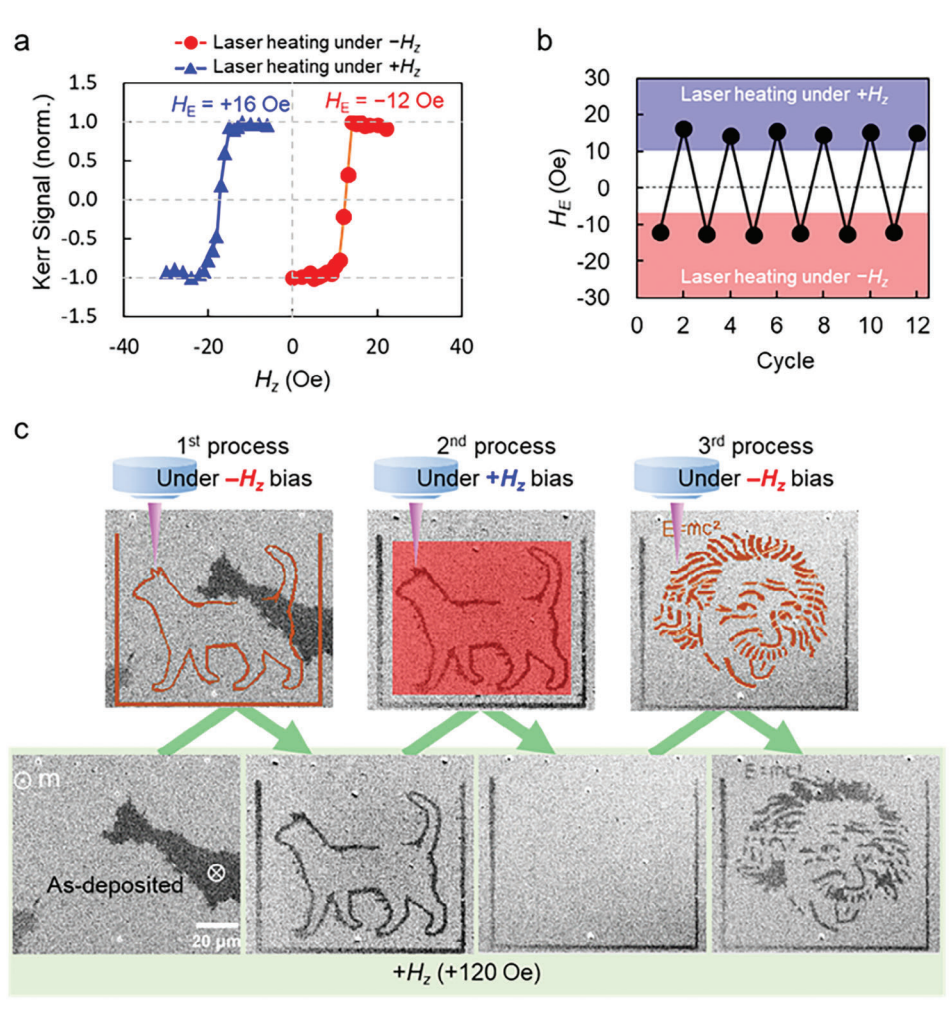


Figure 2. a) Switching of H_E after LFC treatment using laser heating and $\pm H_z$ bias. b) The successive H_E switching. c) Writing-erasing-rewriting function of exchange-biased magnetic patterning in an identical area. Green arrows indicate the order in which the experiments were performed.

the writing-erasing-rewriting capability via our LFC method was demonstrated.

2.3. LDEB Racetrack

In addition to this, we devised an LDEB magnetic DW racetrack in the continuous magnetic film. Figure 3a displays an expansion of the circular up domain under +120 Oe of $H_{\rm z}$ bias in the as-deposited sample as well as LFC at the orange-colored pattern for achieving the DW maze racetrack. As a result of the LDEB patterning, the DW could move along the LDEB maze racetrack, as shown in Figure 3b (the movie is available in the Supporting Information). Note that when the track width is narrow, the speed of the magnetic domain wall tends to slow down because it is relatively more influenced by the track edges (see Figure S3, Supporting Information).

2.4. Current-Driven DW Motion in the LDEB Racetrack

Our LDEB patterning process could be expected to develop functionalities in DW motion-based memory or logic devices. Thus,

we investigated the feasibility of the field- and current-driven DW motion in the LDEB racetrack. To flow a charge current, a 100µm-wide wire-patterned film was fabricated by conventional photolithography (Figure 4a). First, we investigated the field-driven DW motion on the as-deposited multilayer with uniformly inherent positive $H_{\rm E}$ (\approx +75 Oe). Under the positive $H_{\rm z}$ bias, an up domain expanded along the wire in the process of down-up reversal (Figure 4ai-ii); this was shown as natural behavior due to the uniform $H_{\rm F}$ inherent within the overall film surface. Next, LFC was performed on the orange-colored area under $-H_{\nu}$ bias to pattern the Y-shaped racetrack (Figure 4b). After this process, it can be expected that one area corresponding to the inside of the Y shape indicated by the yellow dotted line has a uniformly negative $H_{\rm E}$, whereas other outer areas still retain the positive $H_{\rm F}$. Thus, under +120 Oe of $H_{\rm Z}$ bias during down-up reversal, the up magnetic domain expanded except for the patterned area (Figure 4ci-v).

To investigate the feasibility of the current-driven DW motion along the LDEB Y-shaped racetrack as well as the field-driven DW motion (Figure 4c), a current was injected into an identical wirepatterned sample. Typically, the spin-polarized current is generated because of the spin Hall effect (SHE), where the polarized





www.advelectronicmat.de

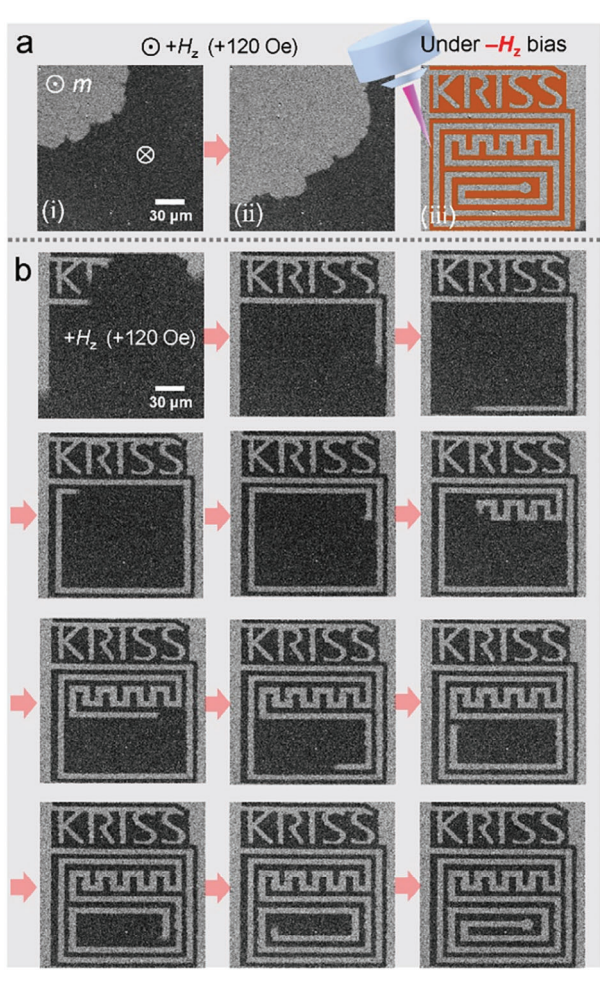


Figure 3. a) MOKE images (i and ii) of up domain expansion of asdeposited sample during down-up reversal, and the image (iii) shows local engineering of $H_{\rm E}$ at the orange-colored pattern for the DW maze racetrack. b) After the process as shown in the image (iii), up expansion, and DW motion along the LDEB maze racetrack, the time interval of each image is 2-s, and the field-driven DW speed is \approx 0.07 mm s⁻¹.

spin (S_P) is proportional to the cross product of the charge current density (j_C) and the spin current vector (j_S) in the Pt layer when a charge current flows through the 100-µm-width wire of a heavy metal Pt layer (Figure 4d). Despite the SHE in IrMn_3, the spin current generated from the bottom Pt layer can be more dominant due to $\approx\!20$ times greater resistivity of IrMn (225.8 µ Ω ·cm) than that of Pt (10.6 µ Ω ·cm). The spin-orbit torque (SOT), induced by injecting S_P into the magnetic layer, can generate an effective magnetic field, H_{SOT} , given by: $^{[4,6,7,16,18,39]}$

$$H_{SOT} = \frac{\hbar \theta_{SH} j_C}{2eM_e t} \left(\mathbf{S}_{P} \times \mathbf{m} \right) \tag{1}$$

where \hbar , θ_{SH} , e, M_s , t, and \mathbf{m} are the Planck constant, spin Hall angle, electron charge, saturation magnetization, magnetic layer thickness, and normalized magnetization direction. By applying Equation (1) into the Néel-Left DW, the H_{SOT} can be induced and can act like a perpendicular external magnetic field along the positive z-axis at the DW center (Figure 4d). Experimental evi-

dence supporting the left-handed Néel DW in our sample structure was shown in Figure S4 (Supporting Information), and the magnitude of H_{SOT} could be obtained from the modulation of the DW dynamics induced by the SOT as shown in Figures S5 and S6 (Supporting Information) (see Section 4; Section S5, Supporting Information for further details). The current-driven DW motion thus becomes possible, and the direction of the motion is illustrated as the green arrow in Figure 4d. Based on the SHE-SOT mechanism mentioned above, the current-driven DW motion along the wire-patterned racetrack was achieved (Figure 4e). By applying several H_z pulses with an amplitude of +100 Oe (0.1s duration), a DW paused at the entrance of the Y racetrack, and then only a current of 40 mA without H_a was injected to move the DW. As a result, the successive images (i-v) of Figure 4e significantly indicate the current-driven DW motion along the Y racetrack. On the other hand, when a negative current of -40 mA was injected along the -y direction, the DW could not move along the opposite direction due to a lack of H_{SOT} to offset inherent H_{E} . Thus, negative H_{r} bias or higher negative current is needed to move DW (see Figure \$7, Supporting Information). Note that, the DW motion can be explained by principles other than the SHE-SOT mechanism, but the SHE-SOT mechanism is the principle that properly explains the direction of DW motion (see Section \$7, Supporting Information for further details).

2.5. Control of Input Channels via LDEB Gate Function

In the present work, we demonstrated field-driven as well as current-driven DW motion based on the LDEB racetrack within continuous magnetic films without using the patterned films shown in Figure 4. Furthermore, we investigated the feasibility of controlling input channels based on selective gating of DW motions (Figure 5). After the procedure of the LDEB Y-shaped racetrack in an identical way as depicted in Figure 4, the gate in the left branch of the Y racetrack was closed by laser heating on a greencolored rectangular area under negative H_z bias (see illustration, Figure 5a). It can be expected that the closed left gate (illustrated by the red-colored rectangular area) and the inside area of the Y shape indicated by the yellow dotted line in Figure 5a have a uniformly negative $H_{\rm E}$, whereas other areas still retain a positive $H_{\rm E}$. Thus, for the field-driven (under +120 Oe of $H_{\rm Z}$ bias during down-up reversal) and the current-driven (injection of +40 mA along the +y axis) DW motions, one DW stopped at the left gate while the other DW moved to the end of the right branch (Figure 5ai-iii). To open the left gate again, laser heating was performed on the green-colored rectangular area under a positive H_{η} bias (see illustration in Figure 5b). After that, successive images (i-iii) of Figure 5b show that the DWs, driven by the field or the current, are well-moved to the ends of both branches. Therefore, we experimentally demonstrated the functionality of the LDEB gate to open or close to pass or stop the DW.

To achieve a logic input representing magnetization states at the end of two branches of the LDEB Y racetrack (illustrated by red squares in Figure 5c), where up-magnetization and down-magnetization are represented as '1' and '0' for digital data, respectively, the two LDEB gates (Gates 1 and 2, Figure 5c) were used within each branch of the Y racetrack. Accordingly, various logic inputs (1,1), (0,1), (1,0), and (0,0) could be realized by



conditions) on Wiley Online Library for rules of use; OA articles are governed by the applicable Creative Commons

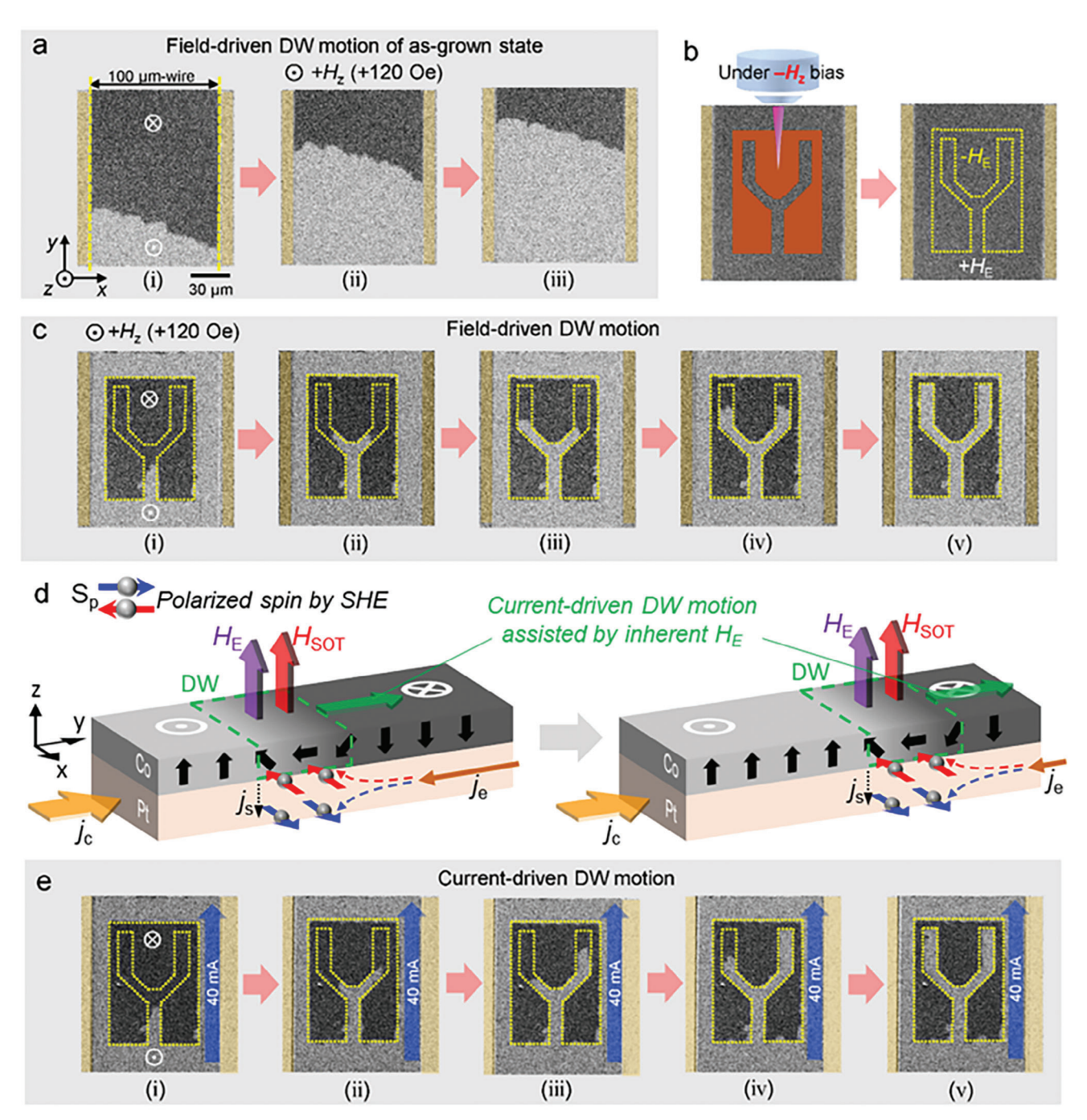


Figure 4. a) Field-driven DW motion in 100- μ m-width wire pattern of the as-deposited sample under +120 Oe of H_z bias during down-up reversal. b) After LFC treatment for the LDEB Y-shaped racetrack; c) field-driven DW motion along the Y-shaped racetrack and the time interval of each image is 500-ms, and the field-driven DW speed is \approx 0.03 mm s⁻¹. d) Illustrations of the spin-polarized current by spin Hall effect (SHE) in the Pt layer and the current-driven DW motion based on the mechanism of spin-orbit torque (SOT). e) Current-driven (40 mA) DW motion along the LDEB Y racetrack, the time interval of each image is 1-s, and the current-driven DW speed is \approx 0.02 mm s⁻¹. In each image, Roman numerals indicate the sequence of state changes.

opening or closing Gates 1 and 2 as magnetization states at the ends of two branches (Figure 5c). These LDEB gates will work well with DW logic devices. The DW logic devices make a uniform magnetization state with a strong magnetic field and go through steps to set the magnetization state of each input termi-

nal. Setting the input magnetization state consumes energy each time. However, the presented LDEB gate is expected to be useful when initializing DW logic devices because no additional energy is consumed unless the set input value is changed. Additionally, by LDEB patterning, multiple branch-shaped racetracks and the

www.advelectronicmat.de

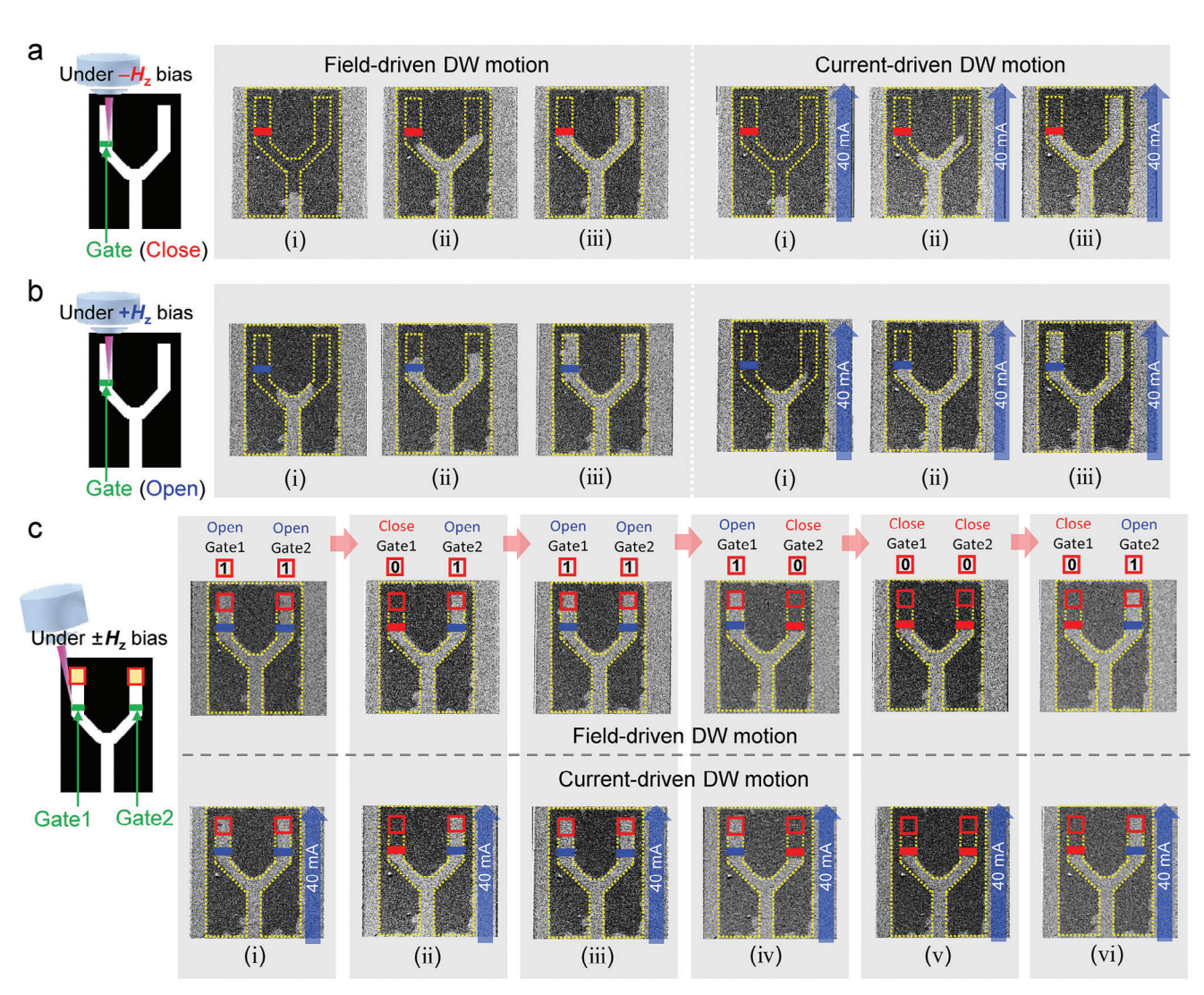


Figure 5. a) Successive images (i–iii) of field- and current-driven DW motion in the LDEB Y racetrack for a closing gate by laser heating under $-H_z$ bias. b) Opening the gate by laser heating under $+H_z$ bias. c) Performance of various inputs by closing or opening the gate using LDEB. In each image, Roman numerals indicate the sequence of state changes.

gate can be expected to facilitate the realization of a demultiplexer function defined as a circuit that can distribute or deliver multiple outputs from a single input.

3. Conclusion

In summary, we have demonstrated in an exchange-coupled system, comprising AFM IrMn $_3$ /FM Co with a Cu space layer, the realization of a reprogrammable $H_{\rm E}$ via LFC using instantaneous irradiation of a laser pulse with a magnetic field bias. This approach allowed for the continuous writing-erasing-rewriting of various exchange-biased magnetic patterns on the same area through local tuning of $H_{\rm E}$, thereby extending its utility as a storage device. Additionally, we showcased the exchange-biased FM DW motion along the LDEB complex racetrack. Moreover, the incorporation of the LDEB gate function within a route of an LDEB racetrack with multiple branches enables the utilization of multiple input channels in next-generation magnetic DW devices. In

future endeavors, it may be plausible to move an exchange-biased skyrmion or bubble along the LDEB racetrack. Furthermore, for practical high DW speed operation in the LDEB racetrack, the injected current density should exceed that of the present work (a few 10¹⁰ A m⁻²). An exploration of the optimal DW speed in the heterogenetic system of AFM and FM will be imperative, involving the control of layer thickness and the substitution of other AFM materials. Previous studies in heavy metal (HM) Pt/FM Co/HM Pt structures have indicated that fine thickness control of the up or down Pt layer can influence DW speed.^[49] In this paper, we utilized an easily accessible visible light microscope to verify the feasibility of LFC, with a resolution limited to ≈ 1 $\mu m.$ To implement local engineering of $H_{\rm E}$ on a smaller scale below a few hundred nm, smaller scale-local engineering of $H_{\rm F}$ can be achieved through thermally assisted magnetic scanning probe lithography (tam-SPL) using a hot tip of a scanning probe microscope. [48] Alternatively, localized field cooling using EUV (Extreme Ultraviolet) light might be another viable method if the



www.advelectronicmat.de

EUV light possesses high energy and generates significant heat. Furthermore, since the magnetic domain wall width of the perpendicular magnetic thin film is $\approx \! 10$ nm, this dimension represents the final limit of device size.

4. Experimental Section

Multilayers of Ti (3 nm)/Pt (3 nm)/Co (0.7 nm)/Cu (1 nm)/IrMn₃ (6 nm)/Pt (2 nm) were deposited on SiO₂ substrates at room temperature by magnetron sputtering with a base pressure of $\approx 1\times 10^{-6}$ torr. To establish a unidirectional and perpendicular $H_{\rm E}$, the deposition process was conducted under a z-axis-external magnetic field ($H_{\rm z}$) oriented in the upward-perpendicular direction with respect to the sample plane.

The magnetic domain, the DW motion, and the magnetic hysteresis loops were observed by the MOKE microscope under an external $H_{\rm z}$ using out-of-plane electromagnets. To obtain a magnetic image, the magnetization state of the FM layer was set as a background image with uniform magnetization in the -z direction, and this background image was subtracted from the observed image. In the magnetic image, the upmagnetization (+z) state of the FM layer appears in light gray, and the down-magnetization (-z) appears in dark gray. The Kerr signal was normalized using the brightness of the up and down states.

To tune $H_{\rm E}$ by the LFC method in a local area, a pulsed laser with a maximum power of 110 mW and wavelength of 660 nm under external $H_{\rm z}$ bias was used on the sample for a duration of 10 ms. However, the actual irradiated laser power on the sample surface through the optical components was 35 mW. This laser power was determined by finding conditions to change the magnetization state without damaging the sample surface (see Figure S8, Supporting Information). The numerical aperture of the objective lens used was 0.6, enabling a spatial resolution of 0.67 µm according to the Rayleigh criterion. However, the measured radius of the focused laser was 0.8 µm (Figure S2b, Supporting Information). This difference was thought to be because the diameter of the parallel beam laser was \approx 3 mm and did not completely fill the aperture of the objective lens.

To find the value of H_z that stops DWs, first H_z was adjusted appropriately so that DWs exist in the observation area. Then, an additional oscillating perpendicular magnetic field was added to the external perpendicular field such as $H_{\rm amp}\sin(2\pi ft)+H_z$. Here, $H_{\rm amp}$ (\approx 200 Oe in this paper) was an amplitude, and f (20 Hz in this paper) was a frequency. $H_{\rm amp}\sin(2\pi ft)$ caused the DWs to move back and forth. If H_z and H_E do not cancel each other out, the overall magnetization state will converge to either the up or down state because the DWs travel different distances back and forth. The up and down states were determined by the sign of H_z+H_E . When H_z and H_E cancel each other out, many DWs can remain, which means that the up domains and the down domains are well mixed. Figure 2a shows the experimental result, and H_E was obtained from the point where the Kerr signal becomes 0 (see Section S9, Supporting Information for further details)

The increase in temperature within the sample was calculated using the COMSOL finite element simulation software according to a laser power of 35 mW. To implement the LDEB magnetic pattering and the LDEB DW racetrack, the laser pulse irradiation was scanned and moved along the patterns by a translation stage (the moving distance along the x-axis or y-axis with a minimum step of 1 μ m). To realize the current-driven DW motion by SHE-SOT, a current of 40 mA was injected into the 100- μ m-width wire-patterned sample using a current source (KEYSIGHT B2901A).

Supporting Information

Supporting Information is available from the Wiley Online Library or from the author.

Acknowledgements

H.-J.K. and K.-W.M. contributed equally to this work. This research was supported by the Nano & Material Technology Development Program

through the National Research Foundation of Korea (NRF) funded by Ministry of Science and ICT (NRF-2021M3F3A2A01037663). K.A. acknowledges support from the National Research Foundation of Korea (NRF) grant (No. 2021R1C1C201226911) funded by the Korean government (MSIT).

Conflict of Interest

The authors declare no conflict of interest.

Data Availability Statement

The data that support the findings of this study are available from the corresponding author upon reasonable request.

Keywords

localized field-cooling, locally different exchange-biased (LDEB) racetrack, local tuning exchange bias field, magnetic domain wall motion, magnetic racetrack

Received: January 12, 2024 Revised: March 21, 2024 Published online: April 3, 2024

- [1] S. Jung, H. Lee, S. Myung, H. Kim, S. K. Yoon, S.-W. Kwon, Y. Ju, M. Kim, W. Yi, S. Han, B. Kwon, B. Seo, K. Lee, G.-H. Koh, K. Lee, Y. Song, C. Choi, D. Ham, S. J. Kim, *Nature* **2022**, *601*, 211.
- [2] D. A. Allwood, G. Xiong, C. C. Faulkner, D. Atkinson, D. Petit, R. P. Cowburn, Science 2005, 309, 1688.
- [3] A. Migliorini, B. Kuerbanjiang, T. Huminiuc, D. Kepaptsoglou, M. Muñoz, J. L. F. Cuñado, J. Camarero, C. Aroca, G. Vallejo-Fernández, V. K. Lazarov, J. L. Prieto, *Nat. Mater.* 2018, 17, 28.
- [4] Z. Luo, A. Hrabec, T. P. Dao, G. Sala, S. Finizio, J. Feng, S. Mayr, J. Raabe, P. Gambardella, L. J. Heyderman, *Nature* 2020, 579, 214.
- [5] G. Yu1, P. Upadhyaya, Y. Fan, J. G. Alzate, W. Jiang, K. L. Wong, S. Takei, S. A. Bender, L.-T. Chang, Y. Jiang, M. Lang, J. Tang, Y. Wang, Y. Tserkovnyak, P. K. Amiri, K. L. Wang, Nat. Nanotechnol. 2014, 9, 548.
- [6] C. K. Safeer, E. Jué, A. Lopez, L. Buda-Prejbeanu, S. Auffret, S. Pizzini, O. Boulle, I. M. Miron, G. Gaudin, *Nat. Nanotechnol.* 2016, 11, 143.
- [7] S. Fukami, T. Anekawa, C. Zhang, H. Ohno, Nat. Nanotechnol. 2016, 11, 621.
- [8] Y.-W. Oh, S.-H. C. Baek, Y. M. Kim, H. Y. Lee, K.-D. Lee, C.-G. Yang, E.-S. Park, K.-S. Lee, K.-W. Kim, G. Go, J.-R. Jeong, B.-C. Min, H.-W. Lee, K.-J. Lee, B.-G. Park, Nat. Nanotechnol. 2016, 11, 878.
- [9] X. Chen, A. Hochstrat, P. Borisov, W. Kleemann, *Appl. Phys. Lett.* 2006, 89, 202508.
- [10] I. L. Prejbeanu, M. Kerekes, R. C. Sousa, H. Sibuet, O. Redon, B. Dieny, J. P. Nozières, J. Phys.: Condens. Matter 2007, 19, 165218.
- [11] J. Nogués, I K. Schuller, J. Magn. Magn. Mater. 1999, 192, 203.
- [12] B. G. Park, J. Wunderlich, X. Martí, V. Holý, Y. Kurosaki, M. Yamada, H. Yamamoto, A. Nishide, J. Hayakawa, H. Takahashi, A. B. Shick, T. Jungwirth, Nat. Mater. 2011, 10, 347.
- [13] C. Y. You, H. S. Goripati, T. Furubayashi, Y. K. Takahashi, K. Hono, Appl. Phys. Lett. 2008, 93, 012501.
- [14] J. Allibe, S. Fusil, K. Bouzehouane, C. Daumont, D. Sando, E. Jacquet, C. Deranlot, M. Bibes, A. Barthélémy, *Nano Lett.* 2012, 12, 1141.
- [15] P. Wadley, B. Howells, J. Železný, C. Andrews, V. Hills, R. P. Campion, V. Novák, K. Olejník, F. Maccherozzi, S. S. Dhesi, S. Y. Martin, T. Wagner, J. Wunderlich, F. Freimuth, Y. Mokrousov, J. Kuneš, J. S. Chauhan, M. J. Grzybowski, A. W. Rushforth, K. W. Edmonds, B. L. Gallagher, T. Jungwirth, Science 2016, 351, 587.







www.advelectronicmat.de

- [16] T. Jungwirth, X. Marti, P. Wadley, J. Wunderlich, Nat. Nanotechnol. 2016, 11, 231.
- [17] P.-H. Lin, B.-Y. Yang, M.-H. Tsai, P.-C. Chen, K.-F. Huang, H.-H. Lin, C.-H. Lai, *Nat. Mater.* 2019, 18, 335.
- [18] H.-J. Kim, S.-G. Je, D.-H. Jung, K.-S. Lee, J.-I. Hong, Appl. Phys. Lett. 2019, 115, 022401.
- [19] J. Yun, Q. Bai, Z. Yan, M. Chang, J. Mao, Y. Zuo, D. Yang, L. Xi, D. Xue, Adv. Funct. Mater. 2020, 30, 1909092.
- [20] X. He, Y. Wang, N. Wu, A. N. Caruso, E. Vescovo, K. D. Belashchenko, P. A. Dowben, C. Binek, *Nat. Mater.* 2010, 9, 579.
- [21] S. M. Wu, S. A. Cybart, P. Yu, M. D. Rossell, J. X. Zhang, R. Ramesh, R. C. Dynes, *Nat. Mater.* 2010, *9*, 756.
- [22] L. Wei, Z. Hu, G. Du, Y. Yuan, J. Wang, H. Tu, B. You, S. Zhou, J. Qu, H. Liu, R. Zheng, Y. Hu, J. Du, Adv. Mater. 2018, 30, 1801885.
- [23] H.-J. Kim, M.-S. Jung, C.-Y. You, J.-I. Hong, *Acta Mater.* **2019**, *171*, 170.
- [24] H.-J. Kim, S. Yoon, J.-H. Ha, W.-C. Choi, J.-I. Hong, Acta Mater. 2021, 210, 116821.
- [25] A. Chen, Y. Zhao, P. Li, X. Zhang, R. Peng, H. Huang, L. Zou, X. Zheng, S. Zhang, P. Miao, Y. Lu, J. Cai, C.-W. Nan, Adv. Mater. 2016, 28, 363.
- [26] M. Liu, J. Lou, S. Li, N. X. Sun, Adv. Funct. Mater. 2011, 21, 2593.
- [27] M. Huang, M. U. Hasan, K. Klyukin, D. Zhang, D. Lyu, P. Gargiani, M. Valvidares, S. Sheffels, A. Churikova, F. Büttner, J. Zehner, L. Caretta, K.-Y. Lee, J. Chang, J.-P. Wang, K. Leistner, B. Yildiz, G. S. D. Beach, Nat. Nanotechnol. 2021, 16, 981.
- [28] J. Zehner, D. Wolf, M. U. Hasan, M. Huang, D. Bono, K. Nielsch, K. Leistne, G. S. D. Beach, Phys. Rev. Materials 2021, 5, L061401.
- [29] J. Zehner, R. Huhnstock, S. Oswald, U. Wolff, I. Soldatov, A. Ehresmann, K. Nielsch, D. Holzinger, K. Leistner, Adv. Electron. Mater. 2019, 5, 1900296.
- [30] P. Vallobra, T. Fache, Y. Xu, L. Zhang, G. Malinowski, M. Hehn, J.-C. Rojas-Sánchez, E. E. Fullerton, S. Mangin, Phys. Rev. B 2017, 96, 144403
- [31] G. Yu, A. Jenkins, X. Ma, S. A. Razavi, C. He, G. Yin, Q. Shao, Q. I. He, H. Wu, W. Li, W. Jiang, X. Han, X. Li, A. C. B. Jayich, P. K. Amiri, K. L. Wang, *Nano Lett.* **2018**, *18*, 980.
- [32] P. Kuświk, M. Matczak, M. Kowacz, K. Szuba-Jabłoński, N. Michalak, B. Szymański, A. Ehresmann, F. Stobiecki, *Phys. Rev. B* 2018, 97, 024404.

- [33] C. L. Chien, V. S. Gornakov, V. I. Nikitenko, A. J. Shapiro, R. D. Shull, Phys. Rev. B 2003, 68, 014418.
- [34] H.-J. Kim, S.-G. Je, K.-W. Moon, W.-C. Choi, S. Yang, C. Kim, B. X. Tran, C. Hwang, J.-I. Hong, Adv. Sci. 2021, 8, 2100908.
- [35] G. Ju, J. Hohlfeld, B. Bergman, R. J. M. van de Veerdonk, O. N. Mryasov, J.-Y. Kim, X. Wu, D. Weller, B. Koopmans, *Phys. Rev. Lett.* 2004, 93, 197403.
- [36] I. Berthold, U. Löschner, J. Schille, R. Ebert, H. Exner, Phys. Procedia 2014, 56, 1136.
- [37] S. Parkin, S.-H. Yang, Nat. Nanotechnol. 2015, 10, 195.
- [38] I. M. Miron, T. Moore, H. Szambolics, L. D. Buda-Prejbeanu, S. Auffret, B. Rodmacq, S. Pizzini, J. Vogel, M. Bonfim, A. Schuhl, G. GaudinFast, Nat. Mater. 2011, 10, 419.
- [39] K. S. Ryu, L. Thomas, S. H. Yang, S. Parkin, Nat. Nanotechnol. 2013, 8, 527.
- [40] S. Emori, U. Bauer, S.-M. Ahn, E. Martinez, G. S. D. Beach, Nat. Mater. 2013, 12, 611.
- [41] M. Baumgartner, K. Garello, J. Mendil, C. O. Avci, E. Grimaldi, C. Murer, J. Feng, M. Gabureac, C. Stamm, Y. Acremann, S. Finizio, S. Wintz, J. Raabe, P. Gambardella, *Nat. Nanotechnol.* 2017, 12, 980.
- [42] K. A. Omari, T. J. Broomhall, R. W. S. Dawidek, D. A. Allwood, R. C. Bradley, J. M. Wood, P. W. Fry, M. C. Rosamond, E. H. Linfield, M.-Y. Im, P. J. Fischer, T. J. Hayward, Adv. Funct. Mater. 2019, 29, 1807282.
- [43] S. Yang, K.-W. Moon, T.-S. Ju, C. Kim, H.-J. Kim, J. Kim, B. X. Tran, J.-I. Hong, C. Hwang, Adv. Mater. 2021, 33, 2104406.
- [44] C. Deger, Nanotechnology 2020, 31, 495209.
- [45] M. Ali, C. H. Marrows, M. Al-Jaward, B. J. Hickey, A. Misra, U. Nowak, K. D. Usadel, *Phys. Rev. B* 2003, 68, 214420.
- [46] H. Xi, R. M. White, J. Appl. Phys. 2003, 94, 5850.
- [47] S. K. Mishra, F. Radu, H. A. Dürr, W. Eberhardt, Phys. Rev. Lett. 2009, 102, 177208.
- [48] E. Albisetti, D. Petti, M. Pancaldi, M. Madami, S. Tacchi, J. Curtis, W. P. King, A. Papp, G. Csaba, W. Porod, P. Vavassori, E. Riedo, R. Bertacco, *Nat. Nanotechnol.* 2016, 11, 545.
- [49] D.-H. Kim, S.-C. Yoo, D.-Y. Kim, K.-W. Moon, S.-G. Je, C.-G. Cho, B.-C. Min, S.-B. Choe, Appl. Phys. Lett. 2014, 104, 142410.



Adv. Electron. Mater. 2024, 10, 2400027